NUCLEAR THEORY, Vol. 38 (2019)
eds. M. Gaidarov, N. Minkov, Heron Press, Sofia

Role of Dinuclear Collective Excitations and Nucleon States in Fusion Dynamics

V.V. Samarin[1,2]

[1]Joint Institute for Nuclear Research, 141980 Dubna, Russia

[2]Dubna State University, 141982 Dubna, Russia

Abstract. Dinuclear vibrational and rotational states of the closely located nuclei and two-center neutron states in the coupled channel approach were used to study fusion dynamics, cross sections and fine structure of the so-called barrier distributions in reactions ^{40}Ca + ^{90}Zr, ^{40}Ca + ^{96}Zr and ^{16}O + ^{154}Sm. The two-center shell model and the time-dependent approach were used for explained of the essential increase of the fusion cross section in the reaction ^{40}Ca + ^{96}Zr as compared with the reaction ^{40}Ca + ^{90}Zr in the vicinity of the Coulomb barrier.

1 Introduction

Two interesting aspects of fusion reactions (e.g. see [1, 2]) are the fine structure of the barrier distribution function (see Figures 1,2)

$$D(E_{\rm c.m.}) = d^2 \left(E_{\rm c.m.}\sigma_{\rm fus}\right)/dE^2_{\rm c.m.} \tag{1}$$

and the increase of fusion cross sections $\sigma_{\rm fus}$ in reactions with some neutron-rich nuclei (see Figure 1a). The well known [3–6] coupled channel method is evolved to include these aspects in the microscopic description by solving two center and time-dependent Schrödinger equations. The method of calculation of the barrier distribution function using cubic splines smoothing is expounded in Section 2.The manifestations of vibration and rotation channels coupling in fusion reactions are studied in Section 3. Role of the two-centered nucleon states in fusion dynamics is studied in the Section 4 using the two-centered shell model and the time-dependent approach.

2 Calculation of Experimental Barrier Distribution Function Using Cubic Splines Smoothing

The function $D(E)$ is ambiguously determined because of experimental errors. To obtain $D(E)$ the mathematically correct procedure of the two-stage spline smoothing proposed in Refs. [7, 8] was used. In the initial stage the smoothing function $f(E) = \ln\left(F(E)\right)$, $F(E) = E\sigma_{\rm fus}(E)$ was found from the condition

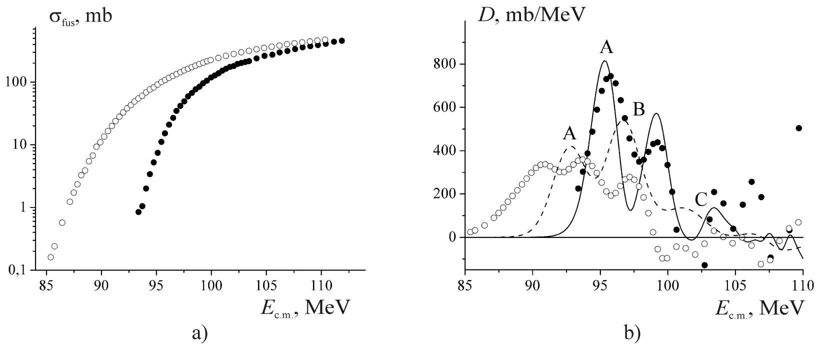

Figure 1. Experimental fusion cross section $\sigma_{\rm fus}(E_{\rm c.m.})$ from Ref. [1] (a) and the barrier distribution function $D(E_{\rm c.m.})$ (b) extracted from this experimental data by cubic spline smoothing in reactions ^{40}Ca + ^{90}Zr (solid circles) and ^{40}Ca + ^{96}Zr (empty circles). The results of calculations of $D(E_{\rm c.m.})$ taking into account vibration coupling for reactions ^{40}Ca + ^{90}Zr (the solid curve) and ^{40}Ca + ^{96}Zr (the dashed curve).

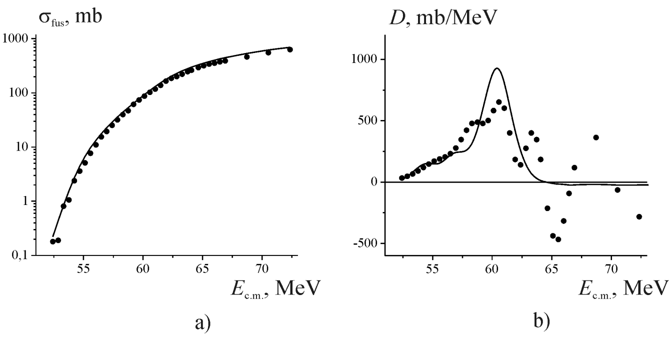

Figure 2. Experimental fusion cross section $\sigma_{\rm fus}(E_{\rm c.m.})$ from Ref. [2] (a) and the barrier distribution function $D(E_{\rm c.m.})$ (b) extracted from this experimental data by cubic spline smoothing in reaction ^{16}O + ^{154}Sm (solid circles). The solid curves are the results of calculations taking into account rotation channels coupling.

of the minimum of the functional [9]

$$\Phi_1\left[f(E)\right]=\int\limits_{E_0}^{E_n}\left[f''(E)\right]^2dE+\sum_{k=0}^{n}p_k^{-1}\left[f(E_k)-f_k\right]^2 \tag{2}$$

with experimental values $f_k=\ln\left(E_k\sigma_{{\rm fus},k}\right)$. The values p_k were found from the conditions

$$|f(E_k)-f_k|\le\Delta\sigma_{{\rm fus},k}/\sigma_{{\rm fus},k}. \tag{3}$$

The barrier distribution function values

$$D_k=F''(E_k)=g'(E_k)\exp\left(g(E_k)\right) \tag{4}$$

and estimations of their errors

$$\delta D_k = |g'(E_k)\exp(g(E_k)) - g_0'(E_k)\exp(g_0(E_k))| \qquad (5)$$

were calculated on the second stage by the smoothing function

$$g(E) = \ln F'(E) = f(E) + \ln f'(E). \qquad (6)$$

It was found from the condition of the minimum of the functional analogous to (2). The function $g_0(E)$ is the result of the calculation without smoothing at the limit $p_k \to 0$. The functions $D(E_{\text{c.m.}})$ for the reactions ^{40}Ca + ^{90}Zr, ^{40}Ca + ^{96}Zr and ^{16}O + ^{154}Sm are shown in Figures 1b,2b. The theoretical results for reactions ^{40}Ca + ^{90}Zr and ^{16}O + ^{154}Sm are similar to the experimental data. The difference between the experimental data and the theoretical curve for reaction ^{40}Ca + ^{96}Zr is consisted in shift to the less values of energy. It may be explained by influence of neutrons excess in ^{96}Zr.

3 The Vibration and Rotation Channels Coupling

The vibration and rotation channel coupling effects in fusion reactions were studied using equations [4–7] for partial channel wave functions $y_{L,\nu}(R)$

$$y''_{L,\nu} - \frac{L(L+1)}{R^2} y_{L,\nu} + \frac{2M}{\hbar^2}\left[E_\nu y_{L,\nu} - \sum_\mu V_{\mu\nu}(R) y_{L,\mu}\right] = 0. \qquad (7)$$

Here L is the orbital momentum of partial wave, M is the reduced mass, $E_\nu = E_{\text{c.m.}} - \varepsilon_\nu$, $E_{\text{c.m.}} = \hbar^2 k_0^2/2M$ is the energy in the center of mass system, ε_ν is the nuclear excitonion energy in the channel ν. $V_{\mu\nu}(R)$ is the coupling matrix for the nucleus-nucleus interaction, R is the internuclear distance. For vibration channels the coupling matrix is $V_{\mu\nu}(R) = \langle\mu|V(R,\beta)|\nu\rangle$ and $|\nu\rangle \equiv \varphi_\nu(\beta)$ are harmonic oscillator functions, $\beta = \{\beta_{i\lambda}\}$, $\beta_{i\lambda}$ is the deformation parameter multipolarity λ. For rotation channels the coupling matrix is $V_{\mu\nu}(R) = \langle\mu|V(R,\theta)|\nu\rangle$, $|\nu\rangle \equiv Y_{l0}(\theta)$ and θ is the angle between the symmetry axis of deformed nucleus (e.g.^{154}Sm) and internuclear axis. The approximate expressions for the functions $V(R,\beta)$, $V(R,\theta)$ with the proximity potential were obtained in [6]. The well-known CCFULL code [4]) (for Woods-Saxon potential) and the code included in the NRV scientific web server [10] for Woods-Saxon and proximity potentials) are often used for the fusion cross section σ_{fus} calculation (see Figure 2a)

$$\sigma_{\text{fus}} = \frac{\pi\hbar^2}{2ME_{\text{c.m.}}j_0}\sum_{L=0}^{\infty}(2L+1)\sum_\nu |j_{L,v}|, \qquad (8)$$

$$j_{Lv} = -i\frac{\hbar}{2M}\left(y_{Lv}\frac{dy^*_{L\nu}}{dR} - y^*_{L\nu}\frac{dy_{Lv}}{dR}\right)|_{R\le R_1+R_2}\,. \qquad (9)$$

Here j_{Lv} is the incoming fusion flux to the compound nucleus region in the channel ν and $j_0 = \hbar k_0/M$. The partial probability density $|\Psi_L(R,\beta)|^2$,

$$\Psi_L(R,\beta) = \sum_{\nu} y_{L,\nu}(R)\varphi_\nu(\beta) \tag{10}$$

for the reaction ^{40}Ca+^{90}Zr, $L = 0$ is shown in Figures 3,4.

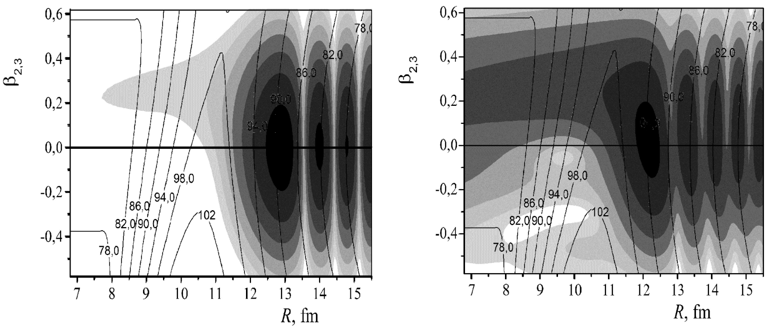

a) b)

Figure 3. The probability density $|\Psi_L(R,\beta_{23})|^2$ flow across the two-dimensional potential barrier $V(R,\beta_{23})$, $\beta_{22} = 0$, $\beta_{12} = 0$, $\beta_{13} = 0$, for the reaction ^{40}Ca + ^{90}Zr, $L = 0$ and energy $E_{\mathrm{c.m.}}$ equal to 92 MeV (a) and 96 MeV (b); R is the internuclear distance; β_{23} is the octupole deformation parameter of the ^{90}Zr nucleus; values of V are shown.

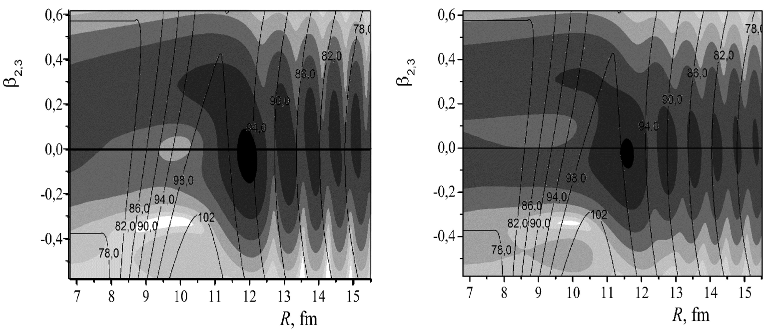

a) b)

Figure 4. The probability density $|\Psi_L(R,\beta_{23})|^2$ flow across the two-dimensional potential barrier $V(R,\beta_{23})$, $\beta_{22} = 0$, $\beta_{12} = 0$, $\beta_{13} = 0$, for the reaction ^{40}Ca + ^{90}Zr, $L = 0$ and energy $E_{\mathrm{c.m.}}$ equal to 98 MeV (a) and 100 MeV (b); R is the internuclear distance; β_{23} is the octupole deformation parameter of the ^{90}Zr nucleus; values of V are shown.

For the energy $E_{\rm c.m.} \leq 96$ MeV near the first peak A in Figure 1b the partial probability density has one jet across the multi-dimensional potential barrier (Figure 3). It is similar to the ground deformation vibrational state. For the energy $E_{\rm c.m.} \geq 98$ MeV near the second peak B in Figure 1b the wave function $\Psi_0(R, \beta)$ has two jets across the multi-dimension potential barrier $V(R, \beta)$ in the (R, β_{23})-plane with $\beta_{22} = 0$, $\beta_{12} = 0$, $\beta_{13} = 0$, (Figure 4). It is similar to the first excited deformation vibrational state. Therefore the barrier distribution may be interpreted using the energy levels $\varepsilon_\alpha(R)$ of the two-surface quadrupole and octupole vibrations of nuclei closely located at the distance R [11]). Energies $\varepsilon_\alpha(R)$ and wave functions $\Phi_\alpha(R, \beta)$ of excited stationary two-surface vibration states can be found from the Schrdinger equation

$$\left[\sum_{i\lambda} H_{i\lambda} + V(R, \beta) - V(R, 0)\right] \Phi_\alpha(R, \beta) = \varepsilon_\alpha(R)\Phi_\alpha. \qquad (11)$$

Where $H_{i\lambda}$ is the Hamiltonian of the independent vibration of the i-th ($i = 1, 2$) nucleus surface, that has a multipolarity λ and $\varepsilon_0(\infty) = 0$. In order to solve approximately the problem specified by Eq. (11), we use an expansion in harmonic oscillator functions. In just the same way as in the coupled channel method [5, 6], we take into account quadrupole and octupole vibrations of both the nuclei, with numbers n_1 and n_2 of corresponding phonons, satisfying the amplitude and energy limitation. The total vibration energy of each nucleus is limited to

$$n_{2i}\varepsilon_{2i} + n_{3i}\varepsilon_{3i} < \Delta\varepsilon_{\max,i}, n = 0, 1, \ldots, i = 1, 2. \qquad (12)$$

Here $\Delta\varepsilon_{\max,i}$ is the upper limit for energies of vibration excitations, that corresponds to their mixing with closely lying non-collective excitations. We used the estimate of the upper limit $\Delta\varepsilon_{\max} \sim \varepsilon_s/2$, where ε_s is the neutron separation energy. Such calculations by the coupled channel method with the proximity potential for the ^{40}Ca+^{90}Zr fusion yield to satisfactory agreement with the experimental data on the cross section $\sigma_{\rm fus}(E_{\rm c.m.})$ and on the barrier distribution $D(E_{\rm c.m.})$ (Figures 1b). Calculated energies $\varepsilon_\alpha(R)$ of modified two-surface vibration states in the ^{40}Ca+^{90}Zr ^{40}Ca+^{96}Zr systems are plotted in Figure 5. In the vicinity of the Coulomb barrier (at a distance $R = R_{\rm B}$) the decrease of energies $\varepsilon_\alpha(R) < \varepsilon_\alpha(\infty)$ accounts for extension deformations of nuclei meeting one another. The spacings $\Delta\varepsilon$ between neighboring vibrational levels depend on R; therefore, in general, excitation energies in the barrier region differ from respective excitation energies in isolated nuclei. In the adiabatic approximation, the potential energy of the nuclear interaction for the modified vibration state with number α can be characterized by the effective potential

$$V_\alpha(R) = V(R) + \varepsilon_\alpha(R), \alpha = 0, 1, \ldots \qquad (13)$$

and by the potential barrier of height $V_{\rm B\alpha}$ at $R = R_{\rm B\alpha}$, which were studied in [11]). Most populated states before the distance of adiabatic potentials (13) are labelled A, B, and C in Figures 5. Peaks of the calculated barrier distribution $D(E_{\rm c.m.})$ (in Figures 1b) correspond to them, and there is a satisfactory similarity between the experimental and calculated distributions for the reaction ^{40}Ca+^{90}Zr in the number of peaks, their relative heights, and the curve shape. The shift of the experimental barrier distribution to the less values of energy for reaction ^{40}Ca + ^{96}Zr may be explained by influence of neutrons excess in ^{96}Zr and neutron transitions with $Q > 0$ (see below).

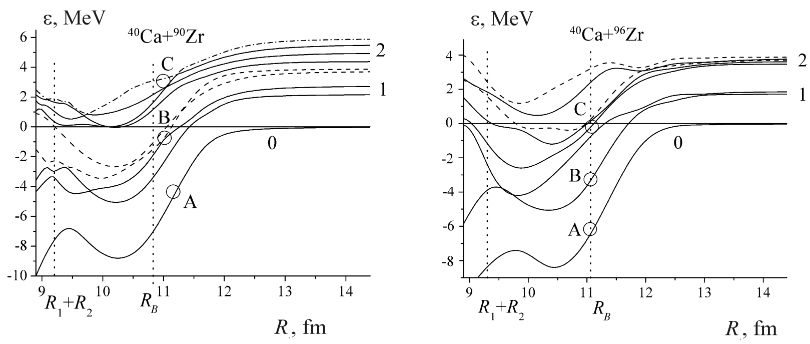

a) b)

Figure 5. Energies $\varepsilon(R)$ of perturbed vibrational levels in the (a) ^{40}Ca + ^{90}Zr and (b) ^{40}Ca + ^{96}Zr systems: curves 0 for ground states, solid curves 1 and 2 for excited states going over to states of zirconium nuclei for $R \to \infty$ (single- and two-phonon states, respectively), dashed and dash-dotted curves for states going over to a superposition of phonons of Ca and Zr nuclei. Points A, B, and C correspond to the most populated states before the barriers of adiabatic potentials, and R_B is the radius corresponding to the vertex of the Coulomb barrier for spherical nuclei of radius R_1 and R_2.

By way of example, we will now consider the ^{16}O nucleus, which is spherical in the ground state, and the deformed nucleus ^{154}Sm at energies in the vicinity of the Coulomb barrier height $V_{\rm B}$. Isolines of the potential relief $V(R,\theta)$ for the ^{16}O + ^{154}Sm system with deformation parameters $\beta_{12} = 0$, $\beta_{13} = 0$ for ^{16}O nucleus and $\beta_{22} = 0.322$ and $\beta_{24} = 0.027$ for ^{154}Sm [2] are shown in Figure 6a. The Coulomb barrier height $V_{\rm B}(\theta)$ for radial motion and the barrier top position $R_{\rm B}(\theta)$ depend on orientation angle θ. As the nuclei being considered approach each other slowly, the spectra $\varepsilon_\alpha(R)$ of rotational states of the ^{154}Sm nucleus and vibrational states of the ^{16}O nucleus change (become perturbed). They can be calculated using a scheme similar to Eqs. (11), (12) for vibrational states. The results for low-lying levels (such that $\varepsilon_\alpha(\infty) < 7$ MeV) of the ^{16}O + ^{154}Sm system are presented in Figure 6b, their properties being determined by the properties of the potential relief $V(R,\theta)$. In the vicinity of the first-barrier top, $R \sim R_{\rm B}(0)$, the potential is weakly dependent on the angle θ (see Figure 6a), while the spectrum of states differs only slightly from the rotational spectrum of an isolated deformed nucleus (see Figure 6b). Rotational

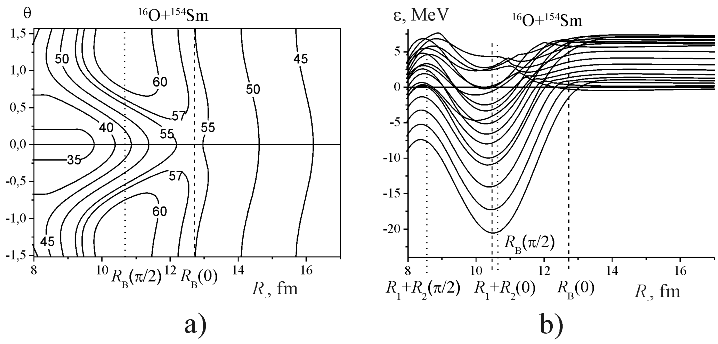

Figure 6. (a) Potential relief for the ^{16}O + ^{154}Sm system and (b) energies $\varepsilon(R)$ of low-lying perturbed collective levels (rotational levels in ^{154}Sm and vibrational levels in ^{16}O). The vertical dashed and dotted lines indicate the radii corresponding to the Coulomb barrier top, $R_B(0)$, and the point at which the nuclear surfaces touch each other, $R_1 + R_2(0)$, in the case, where the prolate nucleus ^{154}Sm is oriented, respectively, along ($\theta = 0$) and across ($\theta = \pi/2$) the axis connecting the centers of colliding nuclei.

levels characterized by high angular momentum values (about a few tens) correspond to energies of a few MeV units. This makes it possible to employ the semiclassical approximation and classical models to describe the behavior of a deformed nucleus. The sudden tunnel approximation is the simplest of such models [1, 2]. Within this model, a deformed nucleus retains a fixed orientation in space in the course of the fusion process. The calculation of the total fusion cross section is based on averaging the penetration of barriers $V(R, \theta)$ close to parabolic ones over the isotropic orientation of the deformed nucleus. This procedure yields results close to experimental data from [2] and to the results of the quantum calculation by the coupled channel method in the so-called no-Coriolis approximation [4–6]. Thus, the application of perturbed collective states provides a substantiation for a classical description of a deformed nucleus and explains the reason behind the proximity of the results produced by the classical and quantummechanical approaches in the region specified by the inequalities $R \geq R_{\rm B}(0)$ and $E_{\rm c.m.} \leq V_{\rm B}(0)$. As the nucleusnucleus distance decreases from $R_{\rm B}(0)$ to $R_{\rm B}(\pi/2)$, the angular dependence of the potential energy $V(\theta)$ resembles ever more closely a nearly parabolic potential well having a deep minimum at $\theta = 0$ (see Figure 6a). Concurrently, perturbed rotational levels also begin resembling harmonic oscillator (nearly equidistant) levels spaced by about 3 MeV (see Figure 6b), which are similar to perturbed vibrational states for two nuclei that are spherical in the ground state (see Figure 5). These states correspond to two-dimensional vibrations or the precession of the symmetry axis of a deformed nucleus about the axis connecting the centers of colliding nuclei. The population of such states at $E_{\rm c.m.} \approx V_{\rm B}(\pi/2)$ in the approximation of the adiabatic potentials (13) also may yield to the formation of a set of maxima spaced by about 3 MeV in the barrier distribution $D(E_{\mathrm{c.m.}})$. As can be seen in Figure 2b, similar weak peaks are observed in processing experimental data. The calculation by the coupled channel method with allowance for dynamical quadrupole and octupole deformations of the ^{16}O nucleus and the static deformation of the ^{154}Sm nucleus reproduces satisfactorily the position and shape of the barrier distribution function $D(E_{\mathrm{c.m.}})$ on the whole and its main peak (see Figures 2b).

4 The Neutron Transfer Channels Coupling

Wave functions $\phi_\alpha(\mathbf{r}, R)$ and energies $\varepsilon_\alpha(R)$ of the valence neutron (with the mass m) of the colliding nuclei may be calculated in the two-center shell model by solving a stationary Schrdinger equation with the potential U and the spin-orbit interaction U_{LS}

$$\left[-\frac{\hbar^2}{2m}\Delta_{\mathbf{r}} + U(\mathbf{r}) + U_{LS}(\mathbf{r})\right]\phi_\alpha(\mathbf{r}; R) = \varepsilon_\alpha(R)\phi_\alpha(\mathbf{r}; R)\,. \qquad (14)$$

The equation (14) was solved by the method based on the series expansion of Bessel functions [12, 14]. The total angular momentum projection $\Omega = \pm 1/2, 3/2, \ldots$ onto the axis connecting the centers of colliding nuclei (the internuclear axis) is the quantum number of two-center states $\varepsilon_\alpha(R) = \varepsilon_{n,\Omega}(R)$, $\phi_\alpha = \phi_{n,\Omega}$. Energies of some two-center (molecular) states in the ^{40}Ca + ^{96}Zr system are plotted in Figures 7a,8a. Neutron transfers from the initial

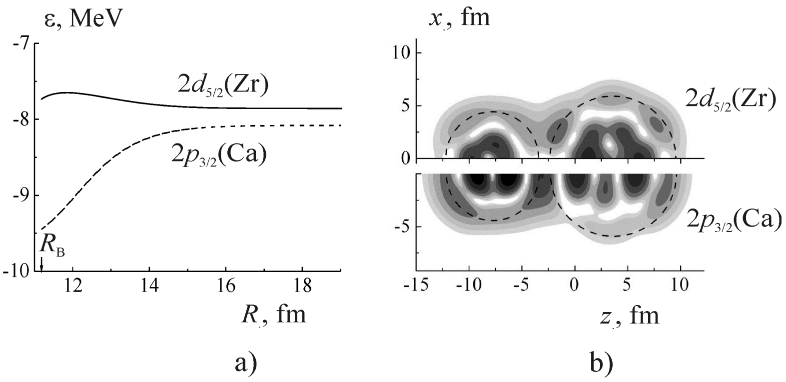

Figure 7. (a) Energies of two-center neutron levels for the absolute values $\Omega = 1/2$ of the total-angular-momentum projection onto the nucleusnucleus axis (z axis) in the ^{40}Ca + ^{96}Zr system that correspond to $2d_{5/2}$ of ^{96}Zr nucleus (solid curve) and $2p_{3/2}$ of ^{40}Ca nucleus (dashed curve); R is the distance between the centers of the nuclei. (b) The probability densities for the two-center states corresponding to the $2d_{5/2}$ of ^{96}Zr nucleus (upper part) and $2p_{3/2}$ of ^{40}Ca nucleus (lower part) for the absolute value of the total-angular-momentum projection onto the nucleusnucleus axis (z axis) $\Omega = 1/2$; arrow indicates the radius of barrier R_{B} for spherical nuclei.

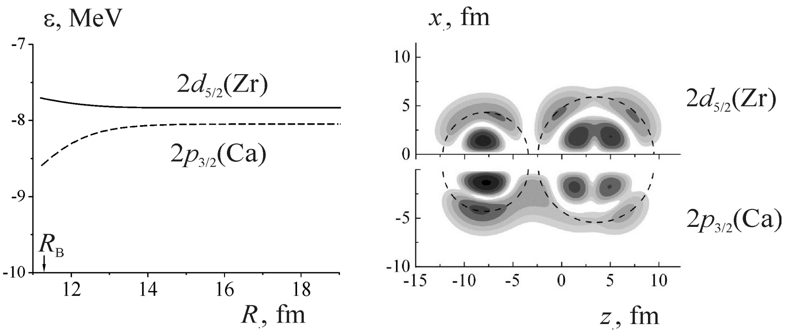

a) b)

Figure 8. Energies of two-center neutron levels (a) and the probability densities (b) for the two-center states in the ^{40}Ca + ^{96}Zr system for the absolute values $\Omega = 3/2$ of the total-angular-momentum projection onto the nucleusnucleus axis (z axis). Table of symbols is even as in Figure 7.

state $2d_{5/2}$ of ^{96}Zr to unoccupied levels $2p_{3/2}$ of ^{40}Ca may yield to an increase in the fusion probability in the reaction ^{40}Ca + ^{96}Zr. Probability densities $|\phi_{n,\Omega}|^2$ for two-center neutron wave functions changed into $2d_{5/2}\left(^{96}\mathrm{Zr}\right)$ and $2p_{3/2}\left(^{40}\mathrm{Ca}\right)$ wave functions in the limit $R \to \infty$ demonstrate a similarity and overlap strongly (see Figures 7b,8b).

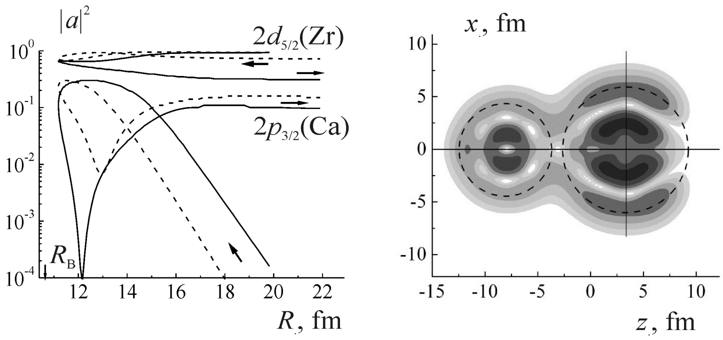

a) b)

Figure 9. (a) The occupation probabilities for the neutron two-center states $2d_{5/2}$ of ^{96}Zr and $2p_{3/2}$ of ^{40}Ca with the absolute value of the total angular momentum projection onto the nucleusnucleus axis (z axis) $\Omega = 1/2$ (solid curve) and $\Omega = 3/2$ (dashed curves) in head-on ^{40}Ca + ^{96}Zr collision at $E_{\mathrm{c.m.}} = 98$ MeV, R is the distance between the centers of the nuclei. (b) Probability density for neutrons of the $2d^6_{5/2}$ outer shell in the ^{96}Zr nucleus (right-hand object) near the turning point in a central collisionwith a ^{40}Ca nucleus (left-hand object) at $E_{\mathrm{c.m.}}$ = 98 MeV; arrow indicates the radius of barrier R_{B} for spherical nuclei.

The occupation probabilities $|a_\alpha|^2$ of the neutron two-center states and neutron probability density for the head-on nucleus-nucleus collision calculated using time-dependent wave functions $\Psi(\mathbf{r}, t)$ [12] are shown in Figure 9. Near the Coulomb barrier the probability of transition from state $2d_{5/2}$ of ^{96}Zr into state $2p_{3/2}$ of ^{40}Ca with pozitive $Q(R)$-value is large. The transition between these two-center energy levels may explain the shift to less energies in the fusion cross section in the reaction ^{40}Ca + ^{96}Zr as compared with the reaction ^{40}Ca + ^{90}Zr.

5 Conclusions

The probability flow across multidimensional barrier for ^{40}Ca + ^{90}Zr fusion shows that peaks of the barrier distribution $D(E_{\rm c.m.})$ correspond to the most populated two-surface vibrational states in vicinity of the barrier. The dynamics of the outer neutron clouds in the time-dependent approach demonstrate that the formation of the two-center nucleon states take place at sub- and near-barrier energies. The transitions between the two-center levels with positive *Q*-values and relatively large probabilities may be a microscopic validation of the empirical coupled channel model and the quantum coupled-channels + empirical neutron rearrangement models [8].

References

[1] H. Timmers, D. Ackerman, S. Beghini *et al.*, *Nucl. Phys. A* **633** (1998) 421-445.

[2] T. Rumin, K. Hagino, N. Takigawa, *Phys. Rev. C* **61** (2000) 014605, 1-11.

[3] V.P. Zhigunov and B. N. Zakharev, *Coupled Channel Method in Quantum Scattering Theory*, Atomizdat, Moscow (1974), in Russian.

[4] K. Hagino, N. Rowley, A.T.Kruppa, *Comp. Phys. Commun.* **123** (1999) 143-152.

[5] V.I. Zagrebaev, V.V. Samarinl, *Nucl. Phys. A* **734** (2004) E9-E12.

[6] V.I. Zagrebaev, V.V. Samarinl, *Phys. At. Nucl.* **67** (2004) 1462-1477.

[7] V.V. Samarin *EPJ Web Conf.* **86** (2015) 00039, 1-4.

[8] A.V. Karpov, V.A. Rachkov, V.V. Samarin, *Phys. Rev. C* **92** (2015) 064603, 1-10.

[9] G.I. Marchuk, *Methods of Numerical Mathematics*, Springer-Verlag, New York (1982).

[10] V.I. Zagrebaev, A.S. Denikin, A.V. Karpov, M.A. Naumenko, V.V. Samarin *et al.*, *NRV Web Knowledge Base on Low-Energy Nuclear Physics*. URL: http://nrv.jinr.ru/.

[11] V.V. Samarin *Phys. of Atom. Nucl.* **72** (2009) 1682-1694.

[12] V.V. Samarin, *Phys. of Atom. Nucl.* **78** (2015) 128-141.

[13] V.V. Samarin, *Phys. of Atom. Nucl.* **78** (2015) 861-872.

[14] V.V. Samarin, *Phys. of Atom. Nucl.* **73** (2010) 1416-1428.